**Edelweiss Applied Science and Technology**
*ISSN: 2576-8484*
*Vol. 8, No. 6, 5490-5501*
*2024*
*Publisher: Learning Gate*
*DOI: 10.55214/25768484.v8i6.3216*


# On-chip implementation of Mach-Zehnder Interferometer (MZI) photonic circuits: Design, simulation and characterization

Arslan Asim[1*], Reza Mokhtarpour[1], Michael Cada[1,2], Yuan Ma[1]
[1]Department of Electrical and Computer Engineering, Dalhousie University, Halifax, NS B3H 4R2, Canada; arslanasim@dal.ca (A.A.), reza.mokhtarpour@dal.ca (R.M.).
[2]Faculty of Materials Science and Technology, VSB-Technical University of Ostrava, 708 00 Poruba, Ostrava, Czech Republic; michael.cada@dal.ca (M.C.).

**Abstract:** As the limitations of integrated electronics start to appear, it becomes important to look for potential alternatives. Silicon photonics holds a lot of promise in this regard. It cannot only provide superior performance to traditional integrated electronics in many aspects, but also co-exist in harmony with it through the realization of electro-optic devices. The focus of this paper is on Photonic Integrated Circuits (PICs) only. A theoretical understanding of Mach-Zehnder Interferometer (MZI) circuits has been developed. Computational design tools have been employed to model photonic waveguides. The design of optical waveguides has been numerically investigated in MATLAB through the Effective Index Method (EIM). The material properties of silicon and silicon dioxide, used in the simulations, have been presented. The properties include the refractive indices, group refractive indices and effective indices. Waveguide geometrical parameters have been explored and a 500 nm x 220 nm silicon waveguide structure has been finalized for experimental work. The schematics for four MZI optical circuits have been prepared in KLayout. Interoperability of KLayout and Ansys Lumerical Interconnect allows for spectral response to be obtained through simulations. The circuits consist of grating couplers, Y-branch splitters and bidirectional couplers. The input signal is split into two waveguide paths. Both waveguide paths culminate into grating couplers connected to photodetectors. The signals from both the channels have been recorded. The fabrication of the chip has been carried out at Applied Nanotools Inc. through Electron Beam Lithography (EBL). The characterization of the devices has been done at 25oC. A decent conformity can be observed between simulation and experimental results.
***Keywords:*** *Lithography, Modeling, Photonic circuits, Silicon on insulator (SOI), Waveguide effective index.*

## 1. Introduction

One of the most astounding achievements of the last century is the development of the field of Integrated Circuit (IC) electronics. In 1965, Moore predicted that the number of transistors on an integrated circuit package would double every year [1]. He later changed the timespan of doubling to 2 years. For decades, the prediction appeared to be valid. Recently, a debate has started on its validity where both sides of the argument have presented their reasoning [2], [3], [4], [5]. The growth of integrated electronics has impacted human lives in unprecedented ways. At this point, as the significance of Moore's law seems to dwindle, it is important to rethink the future growth of integrated devices. One answer is the emerging field of silicon photonics. Around the same time as Moore, Miller proposed the idea of miniaturized optical circuitry, which has been actualized today [6]. Just like integrated electronic circuits drive current around a silicon chip, photonic circuits drive light. The relevance of silicon photonics is paramount, especially as limitations of silicon electronics start to become prominent.

Nanophotonics has natural superiority over nanoelectronics because of the higher speed of light, enabling faster systems. A silicon Photonic Integrated Circuit (PIC) is also more resilient to crosstalk compared to an electronic circuit.


* Correspondence: arslanasim@dal.ca

A major challenge faced by electronic chips is heating and power dissipation, which is not experienced by circuits operating on light. Having mentioned the pros, it is also important to note the cons of photonic circuits. Silicon is not the optimal material for guiding light on a chip. It has long been used in electronic chips.

The semiconductor processes for microelectronics fabrication are well developed. Same processes can be used for the fabrication of photonic chips, which is the reason silicon has been commonly employed for optical circuits. Other challenges include coupling between optical fiber and photonic waveguide, high speed modulators/ detectors and on-chip light sources. Hence, the study of PICs becomes imperative for future growth of semiconductor industry [7], [8], [9].

The components on a silicon photonic chip can mainly be of two types: passive and active. Passive components are used for channeling light on the semiconductor chip. Examples include waveguides, directional couplers and Y-branch splitters. On the other hand, active components are involved in the generation and sensing of light. They may also incorporate electrical and thermal tuning effects. Modulators, detectors and lasers are considered as active components. The work presented in this paper employs passive components on the chip only. The active laser source is not built onto the wafer [10], [11].

In this paper, Mach-Zehnder Interferometer (MZI) designs have been implemented on a Silicon on Insulator (SOI) wafer. Four new variants of unbalanced interferometer circuits have been designed, simulated and fabricated. The design procedure has been carried out in KLayout while simulations have been done in Ansys Lumerical. MATLAB has been used to study propagation characteristics of the waveguides.

To model waveguides, the Effective Index Method (EIM) has been employed. The proposed designs have been fabricated at Applied Nanotools Inc. through Electron Beam Lithography (EBL). Simulation and experimental results have been presented for comparison. PICs hold a lot of promise in cutting-edge technologies and applications like biomedical sensors, optical communications, computing, quantum optics and Artificial Intelligence (AI).

## 2. Theory, Design and Analysis

### *2.1. Waveguide Modeling*

The chip has been implemented on a Silicon on Insulator (SOI) wafer for Transverse Electric (TE) modes [12], [13], [14]. To route light around the semiconductor chip, a three-layered waveguide has been chosen as shown in Figure 1. The waveguide consists of a layer of Silicon (Si) sandwiched between Silicon Dioxide ($SiO_2$).

The silicon waveguide has a thickness of 220 nm. Silicon wafer substrate and buried oxide have approximate thicknesses of 700μm and 2μm, respectively. The waveguide is 500nm wide. In simulations, there are different models that can be employed for modeling the refractive index (n) of Si. The simulation work reported in this paper uses the Lorentz model given below where $\varepsilon = 7.9874$, $\varepsilon_{Lorentz} = 3.6880$ and $\omega_o = 3.9328 \times 10^{15}$.

$$n = \sqrt{\varepsilon + \frac{\varepsilon_{Lorentz}\omega_o^2}{\omega_o^2 - \left(\frac{2\pi c}{\lambda}\right)^2}} \quad (1)$$

*Edelweiss Applied Science and Technology*
*ISSN: 2576-8484*
*Vol. 8, No. 6: 5490-5501, 2024*
*DOI: 10.55214/25768484.v8i6.3216*

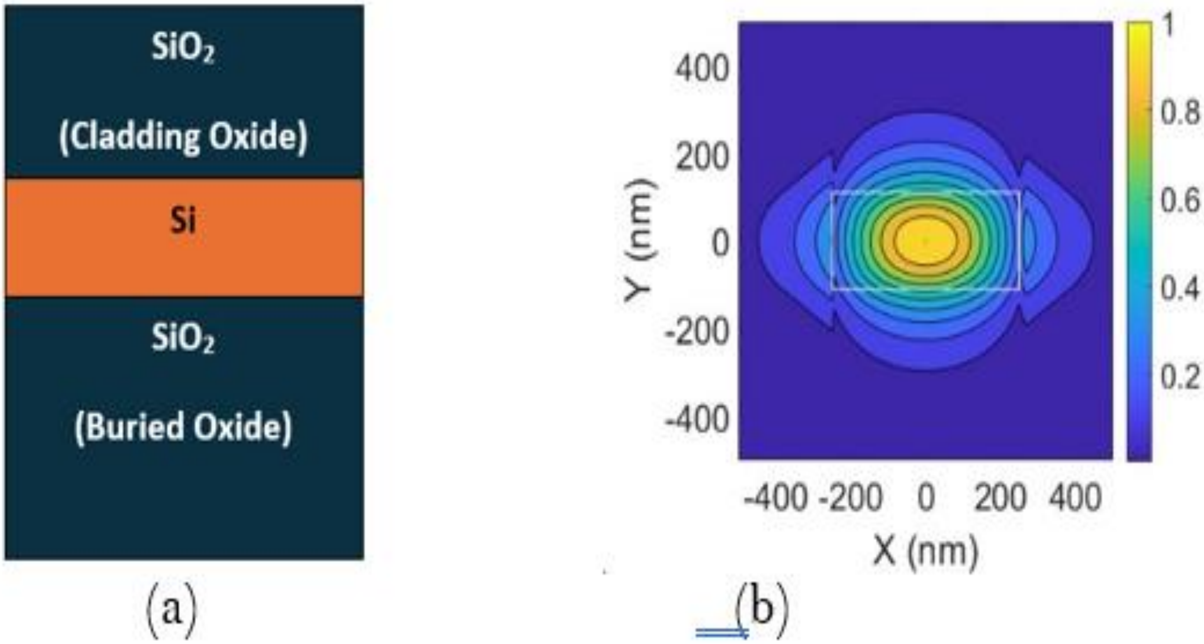


**Figure 1.**
(a) Three-layered waveguide structure. (b) Normalized Electric field (V/m) distribution inside the waveguide.

The field plot in Figure 1 has been generated through the Effective Index Method (EIM). EIM has been implemented in MATLAB. Analytic calculations have been performed to find the 1D out-of-plane Transverse Electric (TE) mode effective index. Similar calculations provide 1D in-plane TM mode effective index. The 1D TE mode effective index is used as input to the TM 1D analytic calculations. The final result is the effective index of the TE mode. The plots in Figures 2 and 3 report the results from 2D EIM. 1 D field profiles can be found through the 1D analytic effective indices. Then, the two 1D field profiles can be multiplied to find the 2D field plot as shown in Figure 1.

The high refractive index contrast between Silicon and Silicon Dioxide helps to ensure that most light is confined within the silicon strip. However, it is important to note that light travels in the form of modes. For a given waveguide geometry, the number of modes needs to be calculated. In the case under consideration, a 500 nm x 220 nm waveguide can carry one mode with good optical confinement, while also seeing some effect of a second mode. The second mode is just starting to appear and hence, very weak. Therefore, the selected waveguide dimensions are suitable for optical circuits. In Figure 1 (b), a strong field can be observed in the center along with some sidelobes. The generation of sidelobes can be attributed to the initiation of the second mode of propagation.

Since refractive index plays a crucial role in waveguide functionality, it is important to touch upon the difference between effective and group refractive indices. The effective index is related to the speed of propagation of a monochromatic beam of light. However, when a pulse propagates through a medium, it experiences temporal broadening. Group velocity becomes more relevant when multiple wavelengths are travelling in a waveguide. Group velocity takes into account the phase velocities of all the wavelengths propagating together. Figure 2 explains how the two types of refractive indices behave with changing wavelengths. The group index remains higher compared to the effective index, which means light travels slower than a monochromatic pulse. The mathematical relationship between effective index and group index is as given below.

$$n_g = n - \lambda \frac{dn}{d\lambda} \qquad (2)$$

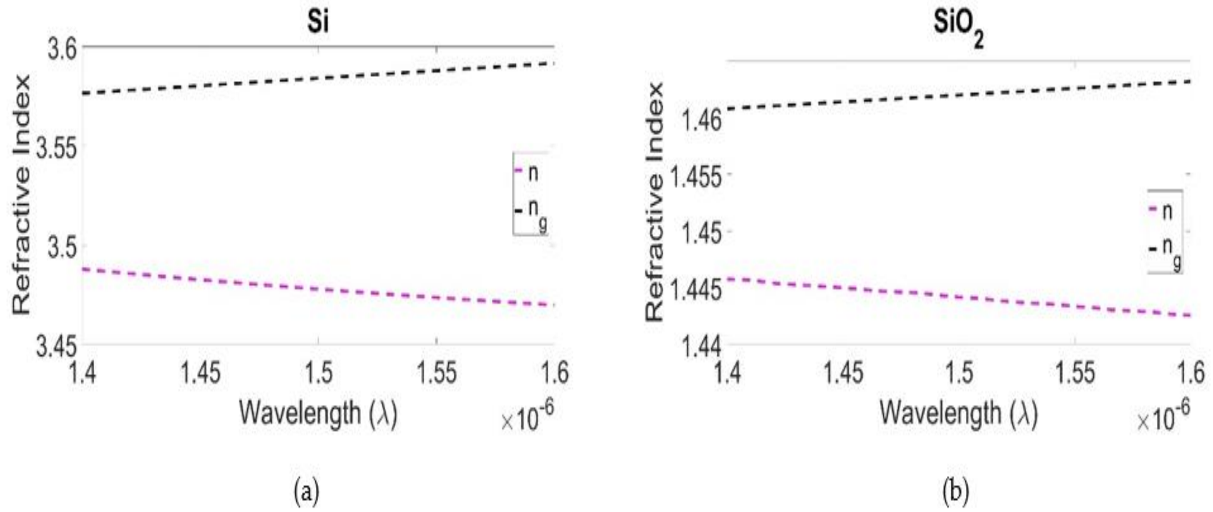


**Figure 2.**
Effective and group refractive indices of (a) Silicon (Si) and (b) Silicon Dioxide ($SiO_2$).

From earlier discussion, it is now established that group velocity and group index are important parameters for waveguide modeling. Equation 2 pinpoints that group index is related to effective index. If the effective index changes, the group index would change as well. This work involves experimental validation, which is prone to device fabrication errors. Thus, it is important to understand how the effective index changes because of fabrication errors. Figure 3 gives an insight into the effective index variation with respect to waveguide geometrical parameters and operating frequencies. Increasing the geometrical parameters of the waveguide also increases effective whereas increasing wavelength causes a decrease in effective index.

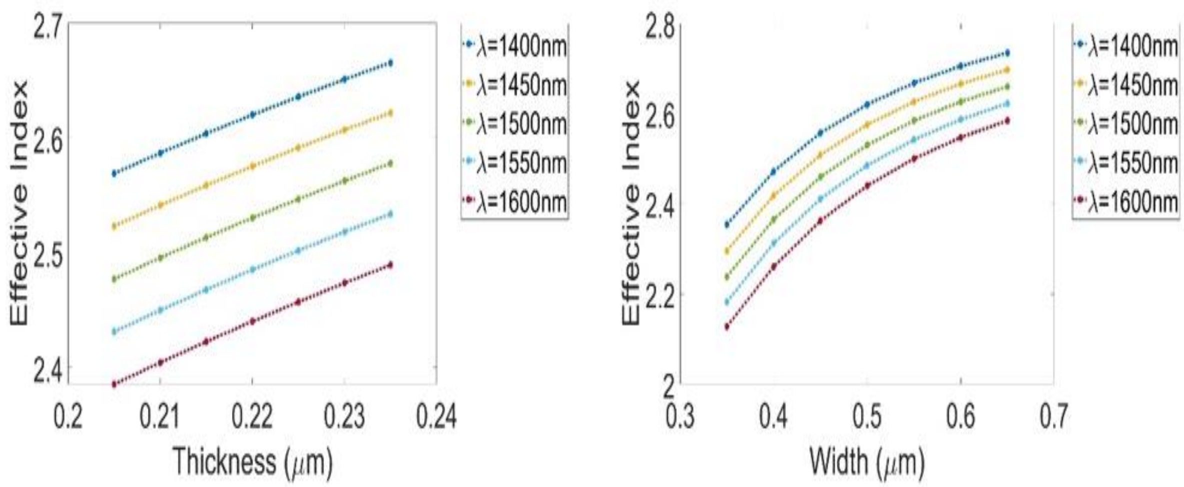


**Figure 3.**
Effect of changing geometrical parameters on waveguide effective indices.

The discussion on effective index above corresponds to Transverse Electric (TE) modes. Since Silicon is a birefringent material, changing the polarization would affect optical constants.

*2.2. MZI Design*

*Edelweiss Applied Science and Technology*
*ISSN: 2576-8484*
*Vol. 8, No. 6: 5490-5501, 2024*
*DOI: 10.55214/25768484.v8i6.3216*

A Mach-Zehnder Interferometer (MZI) is one of the fundamental photonic circuit components. It is the standard choice for on-chip light modulation. It comprises two light paths. If the light paths are of equal lengths, the MZI is balanced. In the case of unequal path lengths, the circuit would be called unbalanced MZI.

Incoming light intensity is equally divided into two channels (in the given case, waveguides). Then light travels through the waveguides undergoing phase change. On the other end, the waveguide paths can again be connected to combine phase effects.

However, in this paper, a different approach has been adopted, which also contributes to the novelty of this work. Light enters the chip through from an optical fiber though a grating coupler and is split into two waveguide arms. Finally, the outcoming beams are routed through grating couplers to two different photodetectors.

In this way, the effect of the arm length difference can be clearly observed. Equations (3) to (8) mathematically explain the behavior of an MZI device in terms of electric fields and intensities.

$$E_1 = \frac{E_i}{\sqrt{2}}, I_1 = \frac{I_i}{2} \quad (3)$$

$$E_2 = \frac{E_i}{\sqrt{2}}, I_2 = \frac{I_i}{2} \quad (4)$$

$$\beta_1 = \frac{2\pi n_1}{\lambda} \quad (5)$$

$$\beta_2 = \frac{2\pi n_2}{\lambda} \quad (6)$$

$$E_{o1} = E_1 e^{-i\beta_1 L_1 - \frac{\alpha_1}{2} L_1} = \frac{E_i}{\sqrt{2}} e^{-i\beta_1 L_1 - \frac{\alpha_1}{2} L_1} \quad (7)$$

$$E_{o2} = E_2 e^{-i\beta_2 L_2 - \frac{\alpha_2}{2} L_2} = \frac{E_i}{\sqrt{2}} e^{-i\beta_2 L_2 - \frac{\alpha_2}{2} L_2} \quad (8)$$

**Table 1.**
Description of mathematical symbols.

| Symbol | Description | Symbol | Description |
|---|---|---|---|
| $I_i$ | Incident light intensity | $E_{o2}$ | Output electric field from waveguide 2 |
| $I_1$ | Intensity in waveguide path 1 | $\alpha_1$ | Waveguide 1 loss |
| $I_2$ | Intensity in waveguide path 2 | $\alpha_2$ | Waveguide 2 loss |
| $E_i$ | Incident beam electric field | $L_1$ | Waveguide 1 length |
| $E_1$ | Electric field in waveguide path 1 | $L_2$ | Waveguide 2 length |
| $E_2$ | Electric field in waveguide path 2 | $n_1$ | Group refractive index of waveguide 1 |
| $\beta_1$ | Propagation constant of waveguide 1 | $n_2$ | Group refractive index of waveguide 2 |
| $\beta_2$ | Propagation constant of waveguide 2 | $\Delta L$ | Difference in MZI waveguide arm lengths |
| $E_{o1}$ | Output electric field from waveguide 1 | $n_g$ | Group refractive index |

Figure 4 presents the layout of the 4 MZIs designed for a Multi-Project Wafer (MPW) run. The allowed chip dimensions are 605 μm by 410 μm. The Silicon Electronic Photonic Integrated Circuits (SiEPIC) Process Design Kit (PDK) has been incorporated into KLayout. Interoperability of KLayout with Ansys Lumerical Interconnect has been established. The description of different device symbols has also been provided in Figure 4 [15], [16], [17].

In each box, the left and right symbols belong to KLayout and Interconnect, respectively. The scheme of the MZI circuit is also highlighted while explaining the symbols. Light entering through the grating coupler at the top is divided into two channels by the Y-branch splitter. A bidirectional coupler, along with waveguides, route light to two different grating couplers, which are connected to detectors.

## 3. Results

An important characteristic of MZI circuit is the Free Spectral Range (FSR), which holds special significance in Wavelength Division Multiplexing (WDM). The FSR of all the MZI circuits is determined numerically and experimentally. Table 2 provides information regarding the difference in arms lengths and simulated/ measured FSRs.

It also highlights the error percentages. All MZI measurements conform well with the simulation results. However, the error is higher for MZI 4. The simulation and experimental results do not completely fit together as well.

This may be due to a number of reasons including fabrication errors, losses in waveguides and noise in the system. Figure 6 provides a complete summary of simulation and experimental results for both output channels of all the MZI circuits. The phase shift between the two channels of each MZI (because of path length difference) is evident as well.

For quantification of noise, measurements are taken between the wavelengths of 1.5 μm and 1.58 μm four times as depicted by Figure 5.

The measurements clarify that the signal-to-noise ratio is good. The mean of the noise remains close to -65 dB. There are outliers in the noise data, shown in red, which have very low magnitudes.

*Edelweiss Applied Science and Technology*
*ISSN: 2576-8484*
*Vol. 8, No. 6: 5490-5501, 2024*
*DOI: 10.55214/25768484.v8i6.3216*

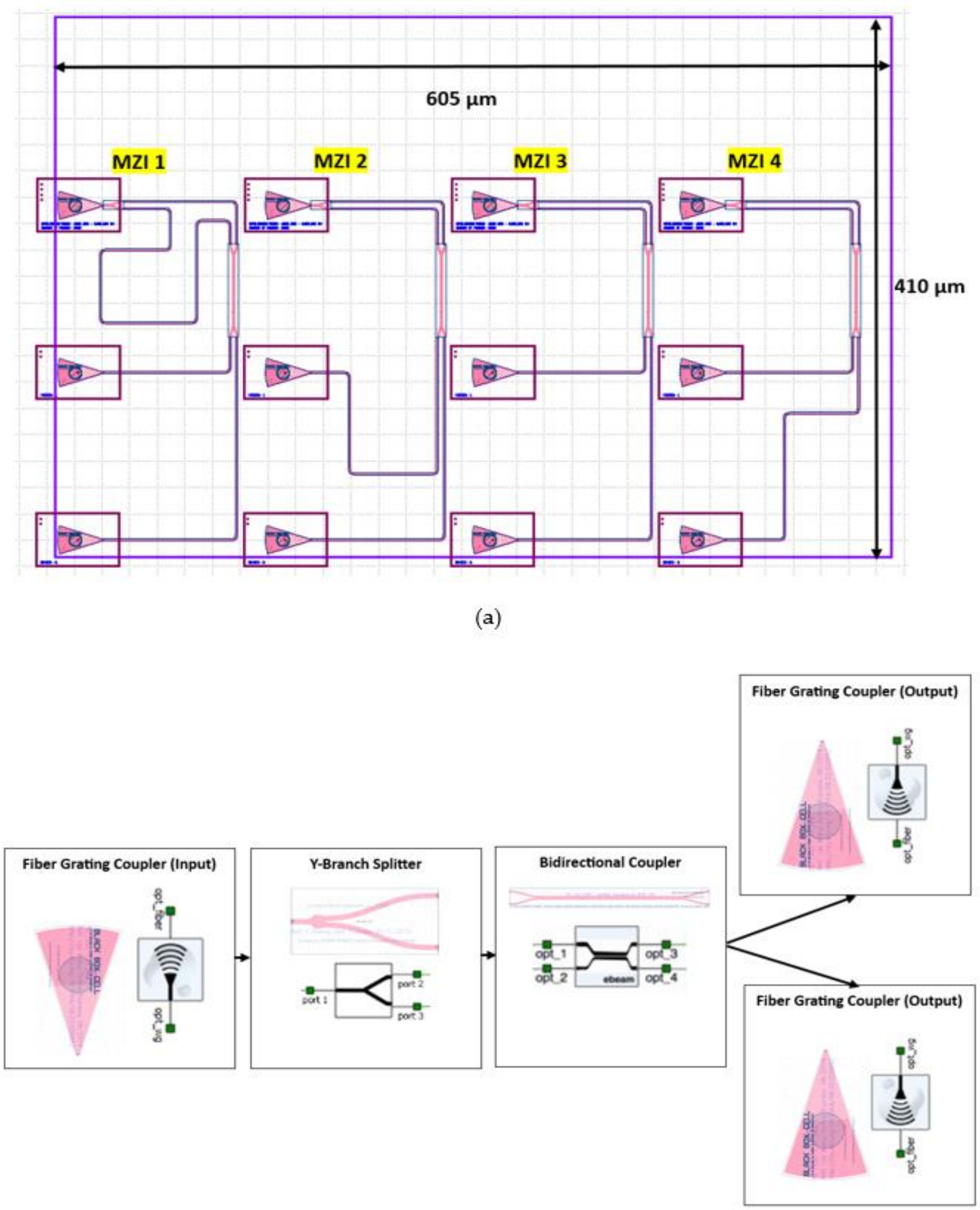


**Figure 4.**
(a) Floor plan of the 4 MZIs created in KLayout. (b) Symbols of the photonic components used in simulations along with description (Left symbol: Klayout, right symbol: Lumerical Interconnect).

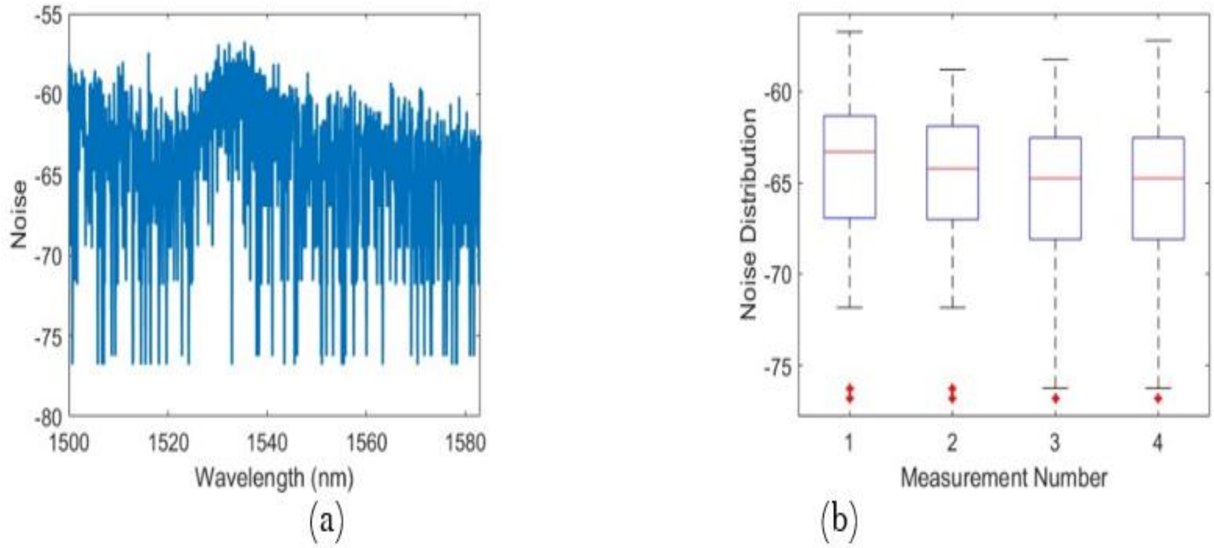


**Figure 5.**
(a) Noise signal. (b) Distribution of noise values between the wavelength of 1.5 μm and 1.58 μm.

**Table 2**.
Free Spectral Ranges (FSRs) of different MZI designs.

| **Device no.** | **\|ΔL\|** | **Simulation FSR** | **Measurement FSR** | **Error =** $\left\|\frac{MEASUREMENT-SIMULATION}{SIMULATION}\right\| X100$ |
|---|---|---|---|---|
| MZI 1 | 105.15 μm | 2.05 nm | 2.00 nm | 2.439 % |
| MZI 2 | 8.877 μm | 1.96 nm | 1.92 nm | 2.041 % |
| MZI 3 | 141.9 μm | 62.00 nm | 60.88 nm | 1.12 % |
| MZI 4 | 138.797 μm | 62.15 nm | 57.28 nm | 7.836 % |

## 4. Fabrication and Measurement

The fabrication of the chip was carried out by Applied Nanotools Inc. based in Edmonton, Alberta through the NanoSOI MPW process. The company used direct-write 100 keV Electron Beam Lithography (EBL) [23]. The diameter of the Silicon on Insulator (SOI) wafer was 200 mm. It was diced into 25 mm x 25 mm square substrates. Initially, the wafer was cleaned with piranha solution (3 $H_2SO_4$: 1 $H_2O_2$).

Then, it was rinsed with water/ Isopropyl alcohol (IPA). After that, hydrogen silsesquioxane (HSQ) was spin-coated onto the substrate. This was followed by heating to evaporate the solvent. The patterning was done at the University of British Columbia using a JEOL JBX-8100FS electron beam instrument.

Tetramethylammonium sulfate (TMAH) solution was then used to develop the pattern. Visual inspection of the devices was carried out to spot defects and residues. The chips were mounted on a 4" handle wafer. They were subjected to an anisotropic ICP-RIE etch process using chlorine. A buffer oxide wet etch was used to remove the resist from the surface. Plasma- Enhanced Chemical Vapor Deposition (PECVD) was used to deposit the cladding oxide with a thickness of 2.2 μm. The deposition procedure was based on tetraethyl orthosilicate (TEOS). It was carried out at 300°C.

For characterization of the circuits, a custom-built automated test setup with automated control software written in Python was used. The measurements were performed using Agilent 81600B tunable laser and Agilent 81635A optical power sensors. A wavelength was used with a step size of 10pm. To ensure TE polarization, a polarization maintaining (PM) fiber was used to supply light to the grating couplers.

**Table 3.**
Comparison of the proposed chip design with contemporary works.

| REF. | NO. OF DESIGNS | $\lambda$ | MAX. FSR | MIN. FSR | FABRICATION |
|---|---|---|---|---|---|
| [18] | 4 | 1.5 - 1.6 µm | 6.56 nm | 0.81 nm | WNF |
| [19] | 5 | 1.5 - 1.6 µm | - | - | ANT and WNF |
| [20] | 7 | 1.5 - 1.6 µm | 14 nm | 3.19 nm | WNF |
| [21] | 2 | 1.2 - 1.3 µm | - | - | IBM |
| [22] | 1 | 1.54 – 1.62 µm | - | - | ANT |
| This work | 4 | 1.5 - 1.6 µm | 62.15 nm | 1.96 nm | ANT |

## 5. Conclusion

In this paper, 4 new MZI circuits have been presented. A complete procedure has been laid out including their theoretical modeling, design specifications and experimental validation. The designs have been investigated using KLayout, Ansys Lumerical and MATLAB. The layout is fabricated by Applied Nanotools Inc. through Electron Beam Lithography (EBL). A comparison has been provided between simulation and experimental results. This work can be extended to applications like optical computing, biophotonic sensing, communications, etc.

The integrated optical circuits provide unique FSR values as well compact size. MZI 3 is of special interest in this regard as it provides a very sharp dips as well as broadband response. The range of FSR values reported in this work is greater than the other recent works as shown in Table 3. The waveguide modeling method used in this work is different compared to other works. An example is [15] which uses different material models. The signals from each of the two MZI channels have also been presented here to show phase difference because of path length differences. This makes it a unique 1x2 circuit. Works like [13] and [16] use other layout strategies. For example, [16] uses 2x2 strategy. Also, characterization of noise floor has hardly been discussed in earlier works.

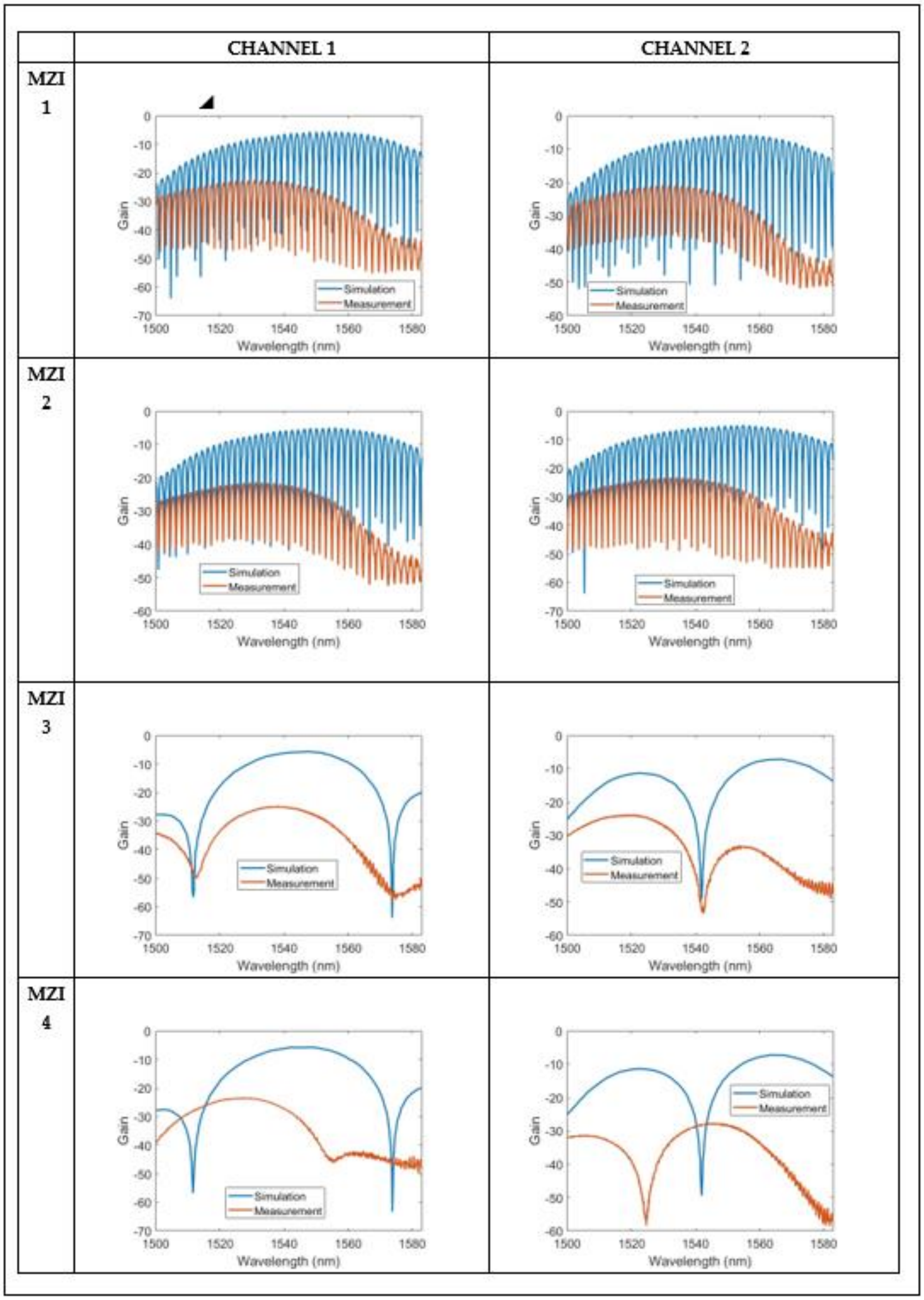


**Figure 6.**
Optical signals received at the two outputs of the MZIs.

## Funding:

This work was supported by NSERC (Natural Sciences and Engineering Research Council) of Canada. Arslan Asim thanks the financial support from Research Nova Scotia and Dalhousie University.

## Acknowledgments:
The course edX UBCx Phot1x Silicon Photonics Design, Fabrication and Data Analysis, which is supported by the Natural Sciences and Engineering Research Council of Canada (NSERC) Silicon Electronic-Photonic Integrated Circuits (SiEPIC) Program, needs special acknowledgement. It was through this course that access to software (Lumerical Solutions, Inc.) and hardware resources became possible. The devices were fabricated by Cameron Horvath at Applied Nanotools, Inc. Iman Taghavi performed the measurements at The University of British Columbia.



## References
[1] G.E. Moore, "Cramming More Components onto Integrated Circuits", Electronics, vol. 38, no. 8, pp. 1-14, 1965.
[2] T. N. Theis and H. P. Wong, "The End of Moore's Law: A New Beginning for Information Technology," Computing in Science Engineering, vol. 19, no. 2, pp. 41–50, mar 2017. [Online]. Available: https://doi.org/10.1109/MCSE.2017.29
[3] C. E. Leiserson, N. C. Thompson, J. S. Emer, B. C. Kuszmaul, B. W. Lampson, D. Sanchez, and T. B. Schardl, "There's Plenty of Room at the Top: What Will Drive Computer Performance after Moore's Law?" Science, vol. 368, no. 6495, jun 2020. [Online]. Available: https://science.sciencemag.org/content/368/6495/eaam9744
[4] M. Horowitz, "Computing's Energy Problem (and What We Can Do About It)," in 2014 IEEE International Solid-State Circuits Conference Digest of Technical Papers (ISSCC). IEEE, feb 2014, pp. 10–14. [Online]. Available: http://ieeexplore.ieee.org/document/6757323/
[5] K. Leswing, "Intel says Moore's law is still alive and well. Nvidia says it's ended," cnbc.com. https://www.cnbc.com/2022/09/27/intel-says-moores-law-is-still-alive-nvidia-says-its-ended.html (accessed Jun. 5, 2024).
[6] S. E. Miller, "Integrated optics: An introduction", Bell Syst. Tech. J., vol. 48, pp. 2059, 1969.
[7] M. Lipson, "Guiding modulating and emitting light on silicon-challenges and opportunities", J. Lightw. Technol., vol. 23, no. 12, 2005.
[8] V. R. Almeida, C. A. Barrios, R. Panepucci and M. Lipson, "All-optical control of light on a silicon chip", Nature, vol. 431, no. 7012, pp. 1081-1084, Oct. 2004.
[9] W. Bogaerts, M. Fiers, and P. Dumon, "Design challenges in silicon photonics," IEEE J. Sel. Topics Quantum Electron., vol. 20, no. 4, Jul./Aug. 2014, Art. no. 8202008.
[10] B. Jalali and S. Fathpour, "Silicon photonics," J. Lightw. Technol., vol. 24, no. 12, pp. 4600–4615, Dec. 2006, doi: 10.1109/JLT.2006.885782.
[11] Z. Yao et al., "Integrated silicon photonic microresonators: Emerging technologies", IEEE J. Sel. Top. Quantum Electron., vol. 24, no. 6, pp. 1-24, Nov./Dec. 2018.
[12] W. Bogaerts and L. Chrostowski, "Silicon photonics circuit design: Methods tools and challenges", Laser Photon. Rev., vol. 12, no. 4, Apr. 2018.
[13] L. Chrostowski and M. Hochberg, Silicon Photonics Design: From Devices to Systems, Cambridge Univ. Press, 2015.
A. Yariv and P. Yeh, Photonics: Optical Electronics in Modern Communications. London, U.K.: Oxford Univ. Press, 2007.
[14] "SiEPIC-EBeam-PDK package for KLayout," Accessed: Nov. 30, 2018. [Online]. Available: https://github.com/lukasc-ubc/SiEPIC_EBeam_PDK
[15] "KLayout," Accessed: Nov. 30, 2018. [Online]. Available: https://www.klayout.de
[16] "SiEPIC-Tools package for KLayout," Accessed: Nov. 30, 2018. [Online]. Available: https://github.com/lukasc-ubc/SiEPIC-Tools
[17] R. S. E. Shamy, A. E. Afifi, M. M. Badr, and M. A. Swillam, "Modelling, characterization, and applications of silicon on insulator loop terminated asymmetric Mach Zehnder interferometer," Sci. Rep., vol. 12, no. 1, Mar. 2022, Art. no. 3598.
[18] Y. Mandke, A. Sivasubramanian, and R. Henry, "Design, Fabrication and characterization of TE Mode MZI Device for Silicon Photonics Integrated Circuit," 2019 IEEE 5th Int. Conf. Converg. Technol. I2CT 2019, no. 7, pp. 1–5, 2019, doi: 10.1109/I2CT45611.2019.9033937.
[19] H. Saghaei, P. Elyasi, and R. Karimzadeh, "Design, fabrication, and characterization of Mach–Zehnder interferometers," Photon. Nanostructures- Fundam. Appl., vol. 37, no. Aug., Aug. 2019, Art. no. 100733, doi: 10.1016/j.photonics.2019.100733.

[20] N. Dupuis et al., "Design and fabrication of low-insertion-loss and low-crosstalk broadband 2 × 2 Mach–Zehnder silicon photonic switches," J. Lightw. Technol., vol. 33, no. 17, pp. 3597–3606, 2015. N. Dupuis et al., "Design and fabrication of low-insertion-loss and low-crosstalk broadband 2 × 2 Mach–Zehnder silicon photonic switches," J. Lightw. Technol., vol. 33, no. 17, pp. 3597–3606, 2015.

[21] Z. Mohammed and M. Rasras, "Robust broadband athermal 2 × 2 Mach–Zehnder interferometer with sub-wavelength grating adiabatic couplers," Opt. Lett., vol. 46, no. 15, p. 3781, 2021, doi: 10.1364/ol.431300.

[22] C. Vieu, F. Carcenac, A. Pépin, Y. Chen, M. Mejias, A. Lebib, L. Manin-Ferlazzo, L. Couraud, and H. Launois, "Electron beamlithography: Resolution limits and applications," Appl. Surf. Sci., vol. 164, nos. 1–4, pp. 111–117, Sep. 2000.4